doi:10.1016/j.jmb.2007.02.006 J. Mol. Biol. (2007) 368, 244–255

JMB

Available online at www.sciencedirect.com
ScienceDirect

ELSEVIER

Folding Kinetics of Staphylococcal Nuclease Studied by Tryptophan Engineering and Rapid Mixing Methods

Kosuke Maki[1], Hong Cheng[1], Dimitry A. Dolgikh[1,2] and Heinrich Roder[1,3]*

[1]*Division of Basic Science Fox Chase Cancer Center Philadelphia, PA 19111, USA*

[2]*Shemyakin-Ovchinnikov Institute of Bioorganic Chemistry, Moscow Russian Federation*

[3]*Department of Biochemistry and Biophysics, University of Pennsylvania, Philadelphia PA 19104-6059, USA*

**Corresponding author*

To monitor the development of tertiary structural contacts during folding, a unique tryptophan residue was introduced at seven partially buried locations (residues 15, 27, 61, 76, 91, 102 and 121) of a tryptophan-free variant of staphylococcal nuclease (P47G/P117G/H124L/W140H). Thermal unfolding measurements by circular dichroism indicate that the variants are destabilized, but maintain the ability to fold into a native-like structure. For the variants with Trp at positions 15, 27 and 61, the intrinsic fluorescence is significantly quenched in the native state due to close contact with polar side-chains that act as intramolecular quenchers. All other variants exhibit enhanced fluorescence under native conditions consistent with burial of the tryptophan residues in an apolar environment. The kinetics of folding was observed by continuous and stopped-flow fluorescence measurements over refolding times ranging from 100 μs to 10 s. The folding kinetics of all variants is quantitatively described by a mechanism involving a major pathway with a series of intermediate states and a minor parallel channel. The engineered tryptophan residues in the β-barrel and the N-terminal part of the α-helical domain become partially shielded from the solvent at an early stage (<1 ms), indicating that this region undergoes a rapid collapse. For some variants, a major increase in fluorescence coincides with the rate-limiting step of folding on the 100 ms time scale, indicating that these tryptophan residues are buried only during the late stages of folding. Other variants exhibit a transient increase in fluorescence during the 10 ms phase followed by a decrease during the rate-limiting phase. These observations are consistent with burial of these probes in a collapsed, but loosely packed intermediate, followed by the rate-limiting formation of the densely packed native core, which brings the tryptophan residues into close contact with intramolecular quenchers.

Keywords: protein folding; continuous-flow; stopped-flow; fluorescence; circular dichroism

Present address: K. Maki, Department of Physics, School of Science, University of Tokyo 113-0033, Japan.

Abbreviations used: H/D, hydrogen/deuterium; SNase, staphylococcal nuclease; WT* SNase, P47G/P117G/H124L variant of SNase; Trp15 SNase, WT* SNase I15W/W140H; Trp27 SNase, WT* SNase Y27W/W140H; Trp61 SNase, WT* SNase F61W/W140H; Trp76 SNase, WT* SNase F76W/W140H; Trp91 SNase, WT* SNase Y91W/W140H; Trp102 SNase, WT* SNase A102W/W140H; Trp121 SNase, WT* SNase H121W/W140H; NATA, *N*-acetyl-L-tryptophanamide; ANS, 8-anilino-1-naphthalene sulfonic acid.

E-mail address of the corresponding author: roder@fccc.edu

Introduction

Elucidating the structural characteristics of transition state ensembles and transient intermediates in protein folding reactions is a key to understanding the mechanisms of protein folding.[1–5] Earlier studies have revealed that small globular proteins often populate compact intermediates with varying degrees of secondary structure within milliseconds of initiating the refolding reaction, long before they encounter the rate-limiting step of the folding reaction.[6–9] Direct observation of the formation of these early intermediates has, however, been difficult mainly due to the limited temporal resolution of conventional mixing devices. Recent advances in ultrarapid mixing and detection methods have made it possible to extend fluorescence and absorbance-detected measurements of solvent-induced refolding reactions into the 10 μs time regime, which has yielded a wealth of new insight into early stages of folding.[10–29] However, detailed structural information on these intermediates, especially with respect to tertiary interactions, is still lacking. Hydrogen/deuterium (H/D) exchange in combination with NMR or mass spectrometry continues to be an important source of information on the structural properties of the folding intermediates at the residue level.[30–34] While quenched-flow H/D exchange methods monitor the formation of hydrogen bonds for backbone amide groups during folding reactions, complementary methods are required that can monitor the development of specific side-chain interactions during early stages of folding. A promising approach to observing individual tertiary interactions relies on the fact that close contact in a folded protein with certain polar amino acids can efficiently quench the fluorescence of tryptophan residues.[35]

Staphylococcal nuclease (SNase) is a 149-residue protein consisting of an N-terminal β-barrel and a C-terminal α-helical subdomain (Figure 1). Although previous studies have indicated that SNase folds to the native state *via* several partially structured intermediates populated along two or more parallel pathways,[24,36–43] little is known about the detailed structural properties of the intermediates. Previous pulsed H/D exchange experiments showed that the amide groups belonging to strands II and III of the β-barrel are already protected within ~10 ms after initiation of folding while the other amides are protected only during the final stages.[37,42] Other studies suggested that the main transition state encountered during SNase folding is a heterogeneous ensemble of states. Mutation analysis revealed that Val66, Ala69 and Ala90 in the β-barrel domain are fully native-like in the transition state.[41] In contrast, the binding sites for Ca^{2+} and an active-site inhibitor, which are located at the interface of the β-barrel and the α-helical domains, are not yet formed at this stage.[43] These findings indicate that the final steps of folding involve formation of specific docking interactions between the subdomains of SNase.

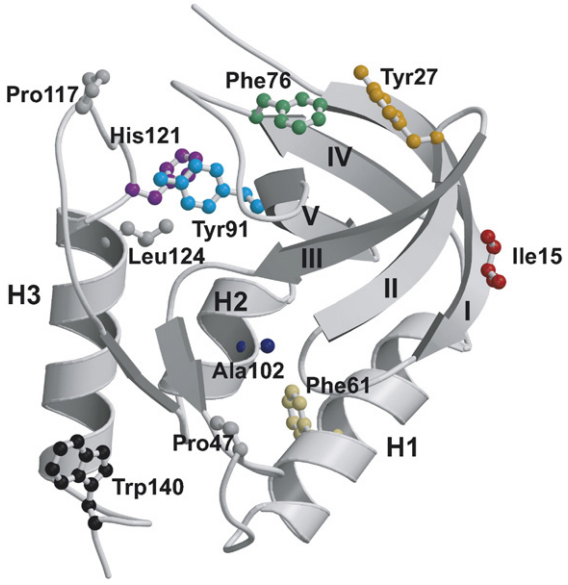

Figure 1. Ribbon diagram of H124L SNase based on the crystal structure.[47] In each of the single-Trp variants of WT* SNase (P47G/P117G/H124L), Trp140 is replaced by His and the following residues are replaced by Trp: Ile15, Tyr27, Phe61, Phe76, Trp91, Ala102 and His121. The five β-strands (I–V) and three α-helices (H1–H3) are labeled. The Figure was prepared using the program MOLSCRIPT.[63]

In an effort to investigate structure formation in the β-barrel domain on the submillisecond time scale, we recently characterized the folding kinetics of the F76W/W140H double mutant of SNase, which contains a sole tryptophan at position 76.[24] Since this residue is largely buried within the β-barrel domain, the fluorescence of Trp76 provides information on the formation of the β-barrel domain, in contrast to Trp140 of the wild-type protein, which reports on the α-helical subdomain. These results suggest that intermediates with a partially formed β-barrel accumulate during an early folding phase with a time constant of 75 μs.[24] Here we explore the equilibrium fluorescence properties and kinetic folding mechanism of six other single-Trp variants, in addition to WT* SNase (P47G/P117G/H124L background) and the Trp76 variant studied previously, in order to gain further insight into the structural characteristics of folding intermediates. The newly engineered tryptophan residues located in the β-barrel and the N-terminal part of the α-helical domain become partially shielded from the solvent, and one of the probes (Trp27) is partially quenched on the submillisecond time scale, indicating that the hydrophobic core and some specific tertiary interactions within the β-barrel are formed during the early stages, but remain uncoupled from the rest of the α-helical domain until the late stages of folding (~100 ms).

Results and Discussion

Single-Trp variants of SNase were constructed by introducing a unique tryptophan residue at various positions throughout the structure into a tryptophan-free background containing P47G, P117G, H124L and W140H mutations.[24] The residues targeted for Trp substitution are Ile15, Tyr27, Phe61, Phe76, Tyr91, Ala102 and His121, which represent most of the secondary structure elements of SNase (Figure 1). The resulting single-tryptophan variants are denoted Trp15, Trp27, Trp61, Trp76, Trp91, Trp102 and Trp121 SNase, respectively.

The thermal unfolding transition of each variant was measured by monitoring the changes in the circular dichroism (CD) spectrum at 222 nm (in 25 mM sodium phosphate, 50 mM sodium chloride, 0.5 mM EDTA, pH 7.0). All variants show a cooperative unfolding transition indicative of a two-state mechanism. Table 1 lists the thermodynamic parameters obtained using standard two-state analysis.[44] The ΔG values range from 3.0 kcal/mol (Trp91 SNase) to 5.2 kcal/mol (Trp121 SNase) at 20 °C and pH 7.0, which is comparable to that of WT* SNase (6.1 kcal/mol), indicating that all variants maintain a native structure of at least moderate stability. On average, the single-Trp variants are destabilized by 1.8 kcal/mol relative to WT* SNase, but the standard deviation around this average is rather small (±0.8 kcal/mol), which facilitates comparison of their kinetic properties. The substitution of His for Trp140 accounts for 0.4 kcal/mol of this destabilization.[24] Table 1 also lists the CD signal at 222 nm (molar mean-residue ellipticity, $[\theta]_{222}$) recorded at 15 °C prior to thermal unfolding scans. All variants show moderately lower $[\theta]_{222}$ ranging from 80% (for Trp91) to 99% (Trp102) of the value for WT* SNase. However, the mutations do not give rise to significant changes in the shape of the CD spectra in the far-UV region (195–250 nm; data not shown for brevity), indicating that they do not alter the overall secondary structure content of the protein. Similar effects have previously been reported for other SNase mutants.[39] A likely explanation for the variation in $[\theta]_{222}$ is that it reflects in part the mutational changes in aromatic residues, which are known to make some contributions to the far-UV CD spectrum.[45]

Fluorescence spectra of WT* SNase and the seven single-Trp variants, along with *N*-acetyl-L-tryptophanamide (NATA) as a reference, were measured at 15 °C under native (100 mM sodium acetate) and denaturing (100 mM sodium acetate, 2.4 M GuHCl) conditions at pH 5.2, and in the acid-denatured state (10 mM phosphoric acid, pH 2), using excitation wavelengths of 280 nm and 295 nm (Figure 2 and Table 2). In the absence of GuHCl, all the spectra exhibit significantly blue-shifted emission maxima (λ_{max} ranging from 323.4 to 341.7 nm) compared to that of NATA ($\lambda_{max} \sim 351$ nm; Table 2), indicating that the tryptophan residues are largely shielded from the solvent in the native state. On the other hand, the fluorescence yields show a great deal of variation among different variants. Trp15, Trp27 and Trp61 exhibit lower fluorescence under native conditions (Figure 2(d)) compared with the corresponding unfolded states (Figure 2(e) and (f)), which can be attributed to specific contacts with polar quenchers in the native structure.[35] Based on the structure of wild-type SNase,[46] likely quenching partners of Trp15, Trp27 and Trp61 are the side-chains of Lys24, Lys28, and Gln106, respectively. Under native conditions, the tryptophan residues at positions 76, 91, 102 and 121 variants exhibit a major enhancement in fluorescence yields (Figure 2(a) and (b)) with respect to the corresponding unfolded states (Figure 2(e) and (f)), indicating that these tryptophan residues are at least partially buried in an apolar, solvent-shielded, environment (see Maki *et al.*[24] with regard to Trp76 SNase). While the fluorescence yield of Trp91 SNase is comparable to that of other proteins when excited at 280 nm (Figure 2(a)), its emission spectrum, normalized with respect to an equimolar solution of NATA, is unusually intense when an excitation wavelength of 295 nm is used (Figure 2(b)). The Trp91 variant also exhibits red-shifted tryptophan absorption and fluorescence excitation spectra (data not shown), which appear to be responsible for its unusual fluorescence properties.

Table 1. Thermodynamic parameters describing the thermal unfolding transitions of WT* SNase and a series of single-Trp SNases (25 mM $NaPO_4$, 50 mM NaCl, 0.5 mM EDTA at pH 7.0) monitored by CD at 222 nm

	$[\theta]_{222} \times 10^{-3}$ (deg cm^2 dmol^{-1})[a]	T_m (°C)	ΔH (kcal/mol)	ΔG (kcal/mol)[b]	$\Delta\Delta G$ (kcal/mol)[c]
WT* SNase[d]	−9.3	66.3	85.2	6.1	0
Trp15 SNase	−8.3	48.3	66.4	3.7	−2.4
Trp27 SNase	−8.1	54.5	72.2	4.5	−1.6
Trp61 SNase	−8.6	53.0	74.6	4.7	−1.4
Trp76 Snase[d]	−8.8	56.6	77.6	5.1	−1.0
Trp91 SNase	−7.7	48.0	58.5	3.0	−3.1
Trp102 SNase	−9.2	53.0	68.0	4.0	−2.1
Trp121 SNase	−8.5	57.0	78.5	5.2	−0.9

[a] Molar mean residue ellipticity at 222 nm at 15 °C measured prior to thermal unfolding scans. The values recorded on the refolded samples after thermal unfolding scans extending up to 70 °C (80 °C for WT*) reproduced the initial reading within error (~5%).
[b] Free energy at 20 °C based on the Gibbs-Helmholtz equation using a constant value of $\Delta C_p = 1.67$ kcal mol^{-1} K^{-1}.
[c] $\Delta\Delta G$ relative to the WT* (WT* = P47G/P117G/H124L).
[d] Values from Maki *et al.*[24]

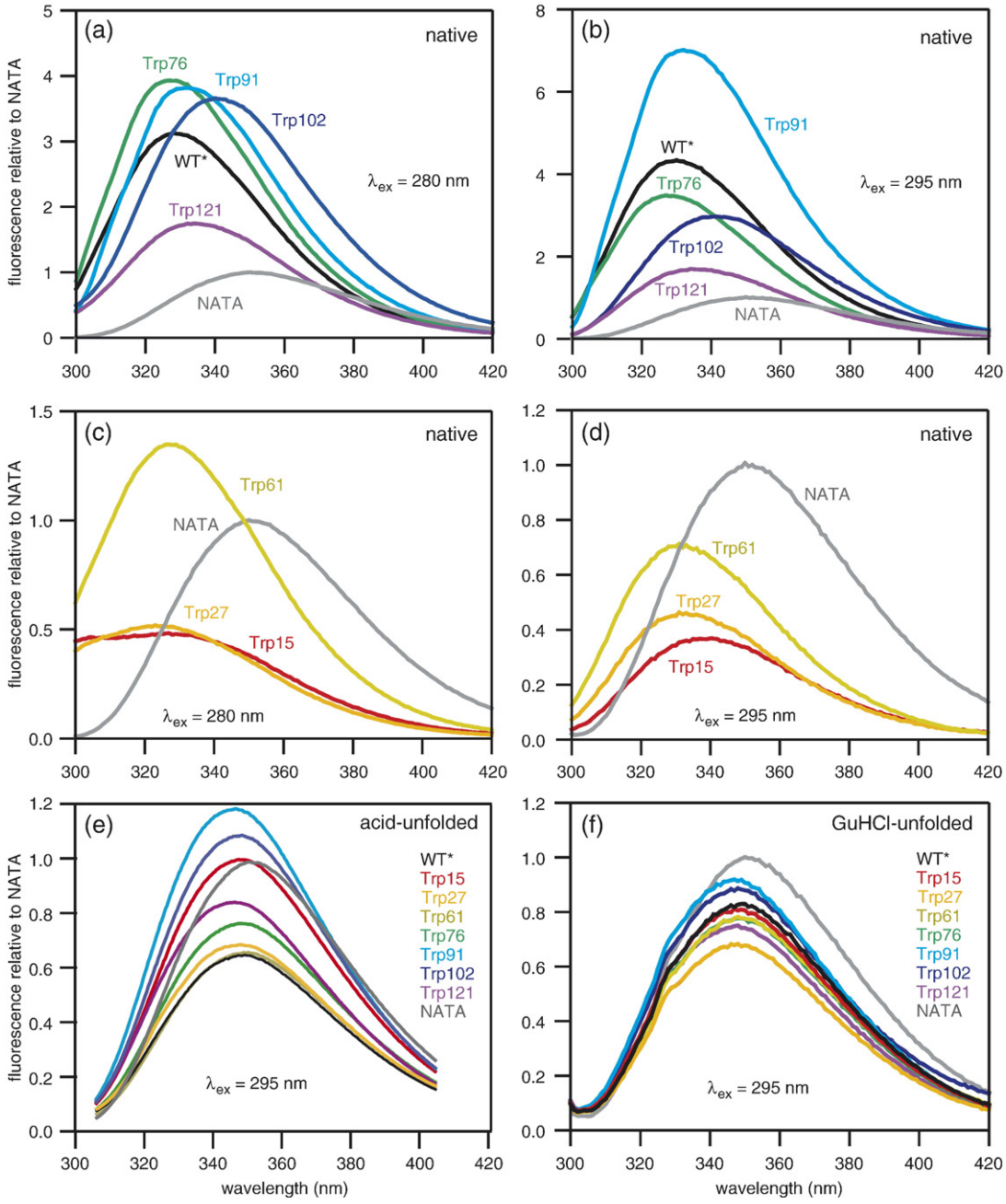

Figure 2. Fluorescence spectra of WT* SNase and single-Trp variants at 15 °C under native and denaturing conditions. Emission spectra of WT*, Trp76, Trp91, Trp102 and Trp121 SNase with excitation at 280 nm (a) and 295 nm (b) in native buffer (100 mM sodium acetate, pH 5.2); emission spectra of Trp15, Trp27 and Trp61 SNase with excitation at 280 nm (c) and 295 nm (d) in native buffer; emission spectra of WT* and all variants (excitation at 295 nm) in 10 mM phosphoric acid at pH 2.0 (e) and in 100 mM sodium acetate, 2.4 M GuHCl, pH 5.2 (f). All spectra are normalized with respect to an equimolar solution of NATA (shown in gray) in the corresponding buffer.

The spectroscopic properties of Trp91 SNase, along with a crystal structure, will be reported elsewhere (K. M., C. Hayden, H. C., Y. C. Park and H. R., unpublished results).

In the presence of 2.4 M GuHCl (Figure 2(f)), the fluorescence spectra of all single-Trp proteins studied are qualitatively similar to that of NATA, and the variation in yield among the different proteins (0.80±0.08) and λ_{max} (347.9±0.7 nm) is much smaller than under native conditions (Figures 2(b)), indicating that the tryptophan residues are fully exposed to the solvent in the unfolded state. The variation in relative yield for the acid-denatured proteins is somewhat larger (0.87±0.21), but λ_{max} exhibits a similar average (347.2 nm) and narrow standard deviation (1.2 nm), indicating that the tryptophan residues are also largely exposed to the solvent in the acid-unfolded form. In the case of Trp27, which exhibits one of the lowest relative yields under native conditions (I_{rel}=0.46), the fluorescence is somewhat depressed even in the acid and GuHCl-denatured state (I_{rel}=0.68–0.69),

Table 2. Fluorescence emission properties of WT* and the single-Trp SNase variants under native (100 mM sodium acetate, pH 5.2), acid-unfolded (10 mM phosphoric acid, pH 2.0) and GuHCl-unfolded (100 mM sodium acetate, 2.4 M GuHCl, pH 5.2) conditions at 15 °C

	Native (pH 5.2)				Acid-unfolded (pH 2)		GuHCl-unfolded (pH 5.2)	
	$\lambda_{ex}=280$ nm		$\lambda_{ex}=295$ nm		$\lambda_{ex}=295$ nm		$\lambda_{ex}=295$ nm	
	I (λ_{max})[a]	λ_{max} (nm)[b]	I (λ_{max})[a]	λ_{max} (nm)[b]	I (λ_{max})[a]	λ_{max} (nm)[b]	I (λ_{max})[a]	λ_{max} (nm)[b]
WT* SNase	3.12	329.2	4.33	330.4	0.65	348.1	0.83	348.7
Trp15 SNase	0.48	326.3	0.37	338.7	1.01	347.5	0.81	347.9
Trp27 SNase	0.52	323.4	0.46	333.1	0.69	347.2	0.68	347.8
Trp61 SNase	1.35	327.8	0.71	331.9	0.66	348.9	0.78	348.7
Trp76 SNase	3.94	327.8	3.48	328.6	0.77	347.9	0.77	348.4
Trp91 SNase	3.82	332.0	7.01	333.0	1.20	345.5	0.92	346.9
Trp102 SNase	3.65	341.0	2.97	341.7	1.10	347.1	0.88	347.6
Trp121 SNase	1.74	334.8	1.69	336.0	0.85	345.5	0.75	347.2
NATA	1.00	351.2	1.00	351.3	1.00	351.1	1.00	351.2

[a] Fluorescence intensity at the emission maximum relative to that of an equimolar solution of NATA in the same buffer.
[b] The wavelength at the emission maximum obtained by non-linear least squares fitting of the fluorescence spectrum in the vicinity of the emission maximum using a Gaussian function.

suggesting that the local Trp27–Lys28 quenching interaction persists in the unfolded state. These residues are part of a reverse turn connecting strands II and III of the native structure (Figure 1), which may be partially formed even under denaturing conditions. Two other tryptophan residues (Trp140 in WT* SNase and Trp61) show evidence for residual quenching at pH 2, and may also participate in residual local interactions with polar residues. In contrast to the data in GuHCl, the acid-denatured forms of two variants (Trp91 and Trp102) show enhanced fluorescence relative to NATA (Table 2), suggesting that these tryptophan residues remain partially shielded from the solvent, perhaps due to (local) clustering of hydrophobic residues.

Taken together, the fluorescence properties of the variants indicate that all seven engineered trptophan residues are largely buried within the native structure and involved in specific tertiary interactions. Along with the observation of cooperative thermal unfolding transitions, our equilibrium analysis confirms that the single-Trp SNase variants maintain the ability to fold into a native-like structure with a close-packed hydrophobic core despite the fact that we replaced partially or fully buried side-chains with a bulky tryptophan.

The refolding reaction of WT* SNase and the single-Trp variants was triggered by a pH jump from 2.0 to 5.2 by tenfold mixing of acid-unfolded protein (in 20 mM phosphoric acid, pH 2.0) with refolding buffer (100 mM sodium acetate, pH 5.3) at 15 °C. The time-course of folding was measured by monitoring tryptophan fluorescence (Figure 3), using a combination of continuous and stopped-flow methods to cover the time range from ~100 μs to ~10 s. The dead times of the continuous and stopped-flow instruments, measured under solvent conditions matching those of refolding experiments, were 100–120 μs and 2.4 ms, respectively. The kinetic traces were fitted to a sum of four to six exponential functions. The kinetic parameters thus obtained are listed in Supplementary Table 1 (see Supplementary Material available on-line). The folding kinetics are similar to those of WT* and Trp76 SNase in terms of the number of kinetic phases and their approximate time constants,[24] indicating that all variants follow a similar folding mechanism. The kinetic scheme of SNase folding proposed on the basis of previous studies on a proline-free variant of this protein,[40] as well as those on WT* and Trp76 SNase,[24] is represented as Scheme 1 (excluding the slow process rate-limited by the isomerization of the peptidyl prolyl bonds; see below):

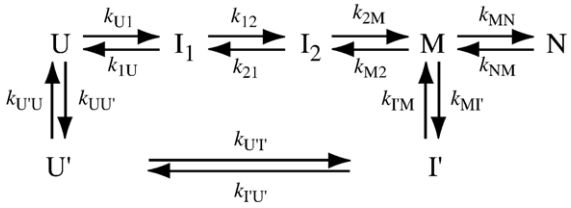

Scheme 1.

where U and U′ represent the unfolded species, while I_1, I_2, I′ and M are intermediate ensembles, and N is the native state. Accumulation of the I_1 state on the major folding pathway is necessary to explain the fastest phase (phase 1 and the corresponding rate constant, λ_1). Accumulation of the I_2 state accounts for a lag phase (phase 3) observed in the ~10 ms time range and the curvature in the chevron plot for the fourth and dominant folding phase (log λ_4 *versus* [urea]).[24] Phase 4 corresponds to the rate-limiting step of the folding reaction, and the curvature is associated with the accumulation of the I_2 state by the relationship $\lambda_4 \sim k_{12}/(k_{12}+k_{21})\times k_{2M}$. Similarly, to account for the curvature of the unfolding limb of the chevron plot reported

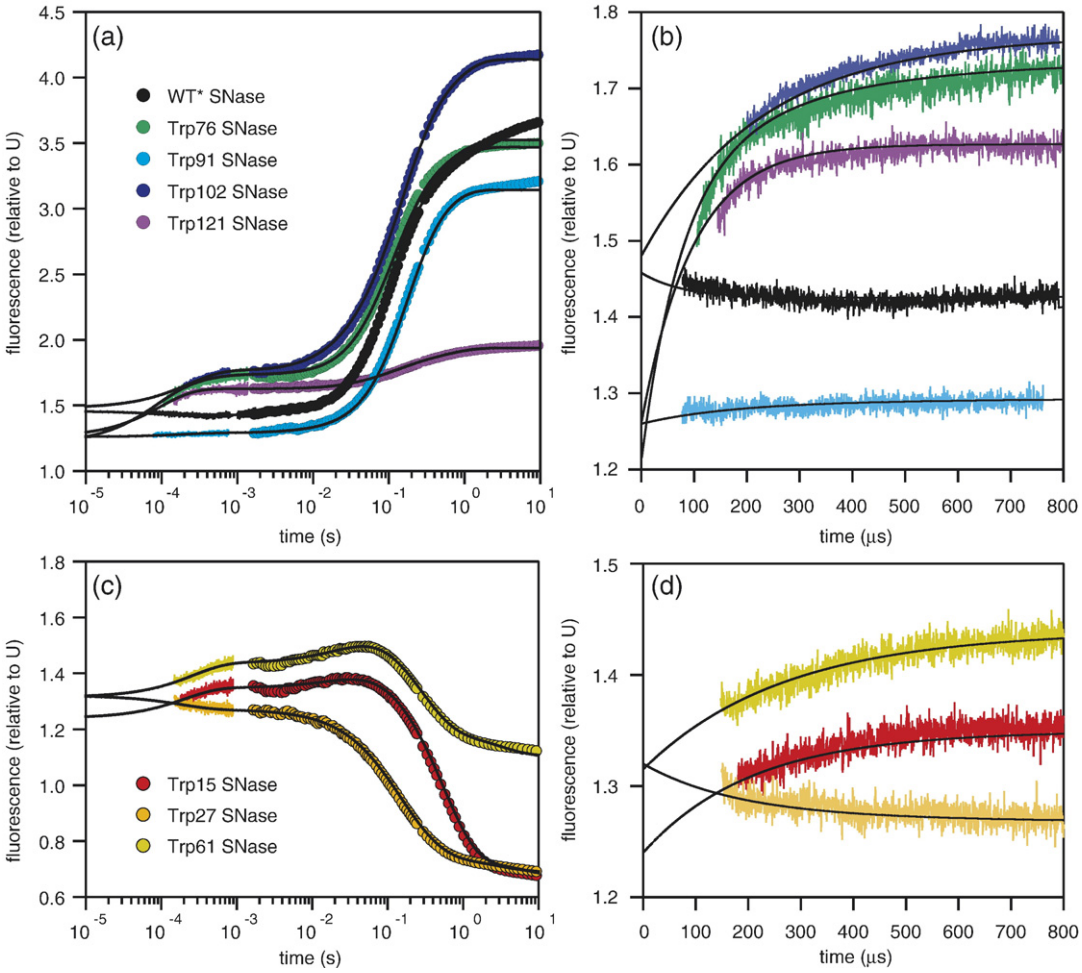

Figure 3. Refolding kinetic traces of WT* SNase and the seven single-Trp variants induced by a pH-jump from 2.0 to 5.2 at 15 °C, measured by the continuous-flow (colored lines) and stopped-flow (circles) methods. (a) and (c) Kinetics of the proteins with enhanced fluorescence (WT*, Trp76, Tpr91, Trp102 and Trp121 SNase) and quenched fluorescence (Trp15, Trp27 and Trp61 SNase), respectively. (b) and (d) Expanded plot of the sub-millisecond time regime measured by the continuous-flow fluorescence. The continuous lines represent the time-courses of folding of these proteins obtained by quantitative kinetic modeling.

previously,[24,40] we introduced a high-energy native-like intermediate, M, which brings about a switch in the rate-limiting step for unfolding ($\lambda_u \sim k_{M2}/(k_{M2} + k_{MN}) \times k_{NM}$; see below). Accumulation of the I′ state along a parallel folding pathway is necessary to account for the second fastest phase (phase 2, λ_2). In addition, a minor phase slower than λ_4 (phase 5, λ_5) is attributed to the interconversion between the I′ and M states (see below).

The slowest phase (phase 6, $\lambda_6 < 0.3$ s^{-1}) of WT*, Trp76, Trp102 and Trp121 SNase arises from a small fraction of molecules folding *via* a parallel pathway that is rate-limited by proline isomerization (typical rate of ~0.01 s^{-1}).[39,40,47] However, the Trp15, Trp27 and Trp61 variants exhibit only five detectable phases. Since the rate of their slowest phase, λ_5, is similar to λ_6 for the remaining proteins, it probably consists of two overlapping events, one of which is rate-limited by the proline isomerization step and the other due to a late step along the minor folding pathway.

Phases 3 and 4 were assigned by using the rate constants and amplitudes of the corresponding phases of WT* and Trp76 SNase as a reference. The phase with the largest change in tryptophan fluorescence (enhancement or quenching, depending on the location of the tryptophan) during folding was assigned to phase 4 ($I_2 \Leftrightarrow M$ step in Scheme 1), whose rate constant ranges from 1.9 s^{-1} (for Trp15 SNase) and 11 s^{-1} (for WT* SNase). As previously reported for WT* and Trp76 SNase,[24] a lag phase with a rate constant λ_3 of 30 to 60 s^{-1}, which corresponds to the $I_1 \Leftrightarrow I_2$ step in Scheme 1, was also observed for the Trp15, Trp61 and Trp102 variants (Trp102 SNase has a somewhat faster lag phase of ~400 s^{-1}; Supplementary Table 1). The characteristic feature of this phase is that the sign of the corresponding amplitude is opposite to that of phase 4, since the fluorescence intensity of the I_2 state is closer to that of the unfolded rather than the native state.[24,40] Although the refolding kinetics of Trp27 SNase lacks a lag phase, the second fastest phase (10.7 s^{-1}) was assigned to phase 3, since the rate of this process is ~3 times faster than λ_4 and comparable to λ_3 of the other proteins.

In addition to these four phases (phases 3–6) observed in the stopped-flow experiments, the continuous-flow fluorescence measurements revealed one (for Trp15, Trp27, Trp61, Trp91, Trp102, Trp121 and WT* SNase) or two (for Trp76 SNase) faster phases for all proteins (Figure 3(b) and (d)), which are assigned to the $U \Leftrightarrow I_1$ and/or $U' \Leftrightarrow I'$ steps in Scheme 1. Distinct changes in fluorescence occur with time constants ranging from 70 μs to 260 μs. Although the amplitude of these rapid phases is smaller than that of the rate-limiting step, the observed fluorescence enhancement nevertheless suggests that the tryptophan side-chains are partially shielded from the solvent in this time regime. The fluorescence change observed in both continuous and stopped-flow experiments fully accounts for the total fluorescence change associated with folding, without evidence for any missing amplitude (burst phase). The fluorescence intensities extrapolated to a refolding time of zero converge to a value between 1.2 to 1.4 on a scale where the fluorescence of the acid-unfolded state is 1, which can be attributed to the fact that the fluorescence intensity of a solvent-exposed tryptophan is ~30% higher at pH 5.2 relative to that at pH 2.0 (measured for NATA at 15 °C). Thus, the initial fluorescence intensity observed here corresponds to that of the unfolded state under refolding condition (pH 5.2 and 15 °C).

The microscopic rate constants (k_{ij}) and the fluorescence intensity of each ensemble were systematically varied until the predicted time-course, based on Scheme 1, reproduced the observed kinetic trace. The kinetic parameters previously determined for WT* and Trp76 SNase served as a starting point in this modeling effort (see Maki *et al.*[24] for a more detailed description of kinetic modeling procedures). The apparent rates and the corresponding amplitudes were determined by numeric calculation of the eigenvalues and eigenvectors of the rate matrix corresponding to Scheme 1. The microscopic rate constants and the fluorescence intensities of each species thus obtained are listed in Tables 3 and 4, respectively. The continuous lines in Figure 3 show the calculated time-course of folding for each variant, which is virtually indistinguishable from the curves obtained by non-linear least-squares fitting of exponentials (data not shown).

A full analysis of the folding mechanism for each variant would require systematic studies as a function of denaturant concentration using multiple spectroscopic probes (e.g. intrinsic and ANS fluorescence), as in our previous analysis of WT* and Trp76 SNase, which is beyond the scope of the present study. However, we were able to obtain reliable estimates of the populations and relative fluorescence yields of the major intermediates encountered during folding by constraining some of the microscopic rate constants defined in Scheme 1 on the basis of our previous work on WT* and Trp76 SNase, which included studies as a function of urea concentration.[24] In cases where two rate constants are mutually coupled, one of them was set to an arbitrary value within a range of possible values. Parameters thus constrained include the back rates k_{1U}, k_{M2}, k'_{IU}, k_{MI} and k_{NM}, as well as the forward rate (k_{MN}), and the interconversion rates between U and U′ ($k_{UU'}$, and $k_{U'U}$). Although most kinetic parameters are close to those previously determined, some of the rates for WT* and Trp76 SNase (k_{U1}, k_{12}, k_{2M} and k'_{IM} of WT*, and k_{U1} and k''_{UI} of Trp76 SNase) were modified slightly in order to improve the fit of the kinetic traces in Figure 3. As in our previous work, we also assumed an arbitrary value of 50,000 s^{-1} for k_{MN}; since the native-like state M is a high-energy intermediate, we can only define the ratio k_{MN}/k_{M2}, based on the roll-over observed in the kinetics of unfolding,[24,40] but the individual rate constants cannot be determined independently. The two unfolded ensembles (U and U′) are assumed to interconvert slowly, so that the major and minor folding pathways are independent of each other during the folding reactions. The two largest rates (λ_1 and λ_2) observed for Trp76 SNase reflect the elementary rate constants k_{U1} and k''_{UI}, respectively. All other variants show only one phase on the

Table 3. Elementary rate constants, k^0_{ij} (s^{-1}), estimated by modeling the folding kinetics of WT* SNase and the single-Trp variants, based on Scheme 1

	WT*	Trp15	Trp27	Trp61	Trp76	Trp91	Trp102	Trp121
$U \rightarrow I_1$	12,000	4800	5400	3700	13,000	5500	4400	10,200
$I_1 \rightarrow U$	(500)[a]	(100)	(100)	(100)	(500)	(100)	(100)	(100)
$I_1 \rightarrow I_2$	28	31	6	23	40	15	390	100
$I_2 \rightarrow I_1$	(25)	(1.5)	(1.5)	(5)	(15)	(5)	(15)	(15)
$I_2 \rightarrow M$	28	1.9	7	4.7	15	13	8	12
$M \rightarrow I_2$	(7.5)	(90)	(90)	(90)	(90)	(90)	(90)	(90)
$M \rightarrow N$	(50,000)	(50,000)	(50,000)	(50,000)	(50,000)	(50,000)	(50,000)	(50,000)
$N \rightarrow M$	(1.8)	(20)	(20)	(20)	(20)	(20)	(20)	(20)
$U' \rightarrow I'$	6500	4800	5400	3700	3800	5500	4400	10,200
$I' \rightarrow U'$	(15)	(100)	(100)	(100)	(100)	(100)	(100)	(100)
$I' \rightarrow M$	2.1	0.12	0.35	0.35	2	2.8	1.9	2
$M \rightarrow I'$	(1)	(0.1)	(0.1)	(0.1)	(0.1)	(0.1)	(0.1)	(0.1)
$U \rightarrow U'$	(4×10^{-5})	(4×10^{-5})	(4×10^{-5})	(4×10^{-5})	(4×10^{-5})	(4×10^{-5})	(4×10^{-5})	(4×10^{-5})
$U' \rightarrow U$	(0.001)	(0.001)	(0.001)	(0.001)	(0.001)	(0.001)	(0.001)	(0.001)

[a] Rate constants in parentheses are poorly defined on the basis of kinetic data in the absence of denaturant; they were set to the corresponding rate constants for WT* and Trp76 SNase determined previously,[24] or set arbitrarily within a range of allowed values.

Table 4. Fluorescence intensity of each state relative to the acid-unfolded state estimated by modeling the folding kinetics of WT* and the single-Trp variants, based on Scheme 1

	Fluorescence intensity relative to the acid-unfolded state							
State	WT* SNase	Trp15 SNase	Trp27 SNase	Trp61 SNase	Trp76 SNase	Trp91 SNase	Trp102 SNase	Trp121 SNase
U	1.47	1.24	1.32	1.32	1.21	1.26	1.48	1.26
I_1	1.42	1.35	1.27	1.44	1.75	1.29	1.77	1.63
I_2	1.5	1.43	0.6	1.65	1.8	1.5	1.77	1.63
M	3.47	0.65	0.69	1.1	3.5	3.15	4.15	1.93
N	3.47	0.65	0.69	1.1	3.53	3.15	4.15	1.93
U′	1.43	1.24	1.32	1.32	1.21	1.26	1.48	1.26
I′	1.43	1.35	1.27	1.44	1.75	1.29	1.77	1.63

submillisecond time scale (see Supplementary Table 1), indicating that the initial collapse rate for both the major and minor unfolded species are similar ($k_{U1} \approx k_{UI}'$). This conclusion is consistent with the observation that all variants exhibit a minor slow phase (phase 5) assigned to refolding of a heterogeneous I′ ensemble, and thus explains the presence of a rapid process corresponding to interconversion between U′ and I′ ensembles. Although WT* SNase shows only a small decrease in fluorescence on the submillisecond time scale (Figure 3(b)), the k_{U1} value obtained is consistent with our previous study using ANS fluorescence.[24]

After manually optimizing the elementary rate constants to reproduce the observable rates (see Supplementary Data, Table 1), the intrinsic fluorescence of each state was adjusted so that the time-course calculated from the microscopic rate constants fully reproduces the experimentally obtained kinetic traces (Figure 3). The fluorescence values for each state, normalized with respect to the acid-unfolded state at pH 2, are listed in Table 4. As mentioned above, the values for the U-state are larger than 1, since they reflect the unfolded ensemble under refolding conditions (pH 5.2) resulting in ~30% higher fluorescence compared to pH 2. The fluorescence of the native-like high-energy intermediate M, whose spectroscopic properties cannot be measured directly, was assumed to be the same as that of the N state.[40] This modeling procedure led to an excellent fit of the observed kinetic trace for each variant studied (Figure 3), indicating that Scheme 1 is consistent not only with WT* and Trp76 SNase,[24] but also describes the folding mechanism of all other single-tryptophan variants studied here.

Our comprehensive set of kinetic parameters and relative fluorescence values for the different tryptophan probes (Tables 3 and 4) provides new insight into the structural characteristics of the intermediates populated during SNase folding. While the variants studied previously lacked appropriate optical probes for monitoring the rapid formation of the β-barrel domain, we now have unique fluorophores in different locations (Figure 1) that allow us to monitor the formation of the β-barrel and the α-helical domains. For several variants (Trp15, Trp61, Trp76, Trp91, Trp102 and Trp121), the I_1 and I′ states populated on the 100 μs time scale exhibit enhanced fluorescence compared with the unfolded ensembles (Table 4). Since the fluorescence emission spectra under denaturing conditions (Figure 2(e) and (f)) indicate that all tryptophan residues are largely exposed to the solvent in the unfolded state, the initial increase in the fluorescence intensity is likely to reflect partial protection of the tryptophan side-chains from the solvent in the I_1-state (the same is true for the I′ state populated along a minor parallel pathway, but for simplicity we will focus on the major pathway). A rapid increase in fluorescence on the submillisecond time scale was reported for several other proteins, including the bacterial immunity protein Im7 and single-Trp variants of ubiquitin and ribonuclease A, and was also attributed to partial burial of a tryptophan residue within the hydrophobic core.[17,25,48] In the present study, we have observed a rapid fluorescence enhancement for several individual tryptophan probes in different locations throughout the SNase structure (Figure 1), including the β-barrel domain (strands I, IV, V and helix H1) and parts of α-helical domain (helix H2 and the N terminus of helix H3), suggesting that a major portion of the chain undergoes a cooperative collapse within ~100 μs of initiating the folding reaction. This result is fully consistent with the previous folding experiments on WT* and Trp76 SNase monitored *via* the hydrophobic dye ANS, which revealed the formation of a loosely packed hydrophobic core in the same time regime.[24]

The three variants that experience intramolecular fluorescence quenching under native conditions (Figure 3(c)) are especially informative. While the fluorescence of Trp15 and Trp61 SNase is enhanced in the I_1 state compared to both U and N states, Trp27 SNase shows a small, but clearly detectable, decrease in fluorescence during the initial folding phase (Figure 3(d)). In fact, Trp27 SNase is the only one among all single-Trp variants studied with a lower intrinsic fluorescence in I_1 relative to U (Table 4), indicating that Trp27 comes in contact with an intramolecular quencher; a likely candidate is Lys28, which is within 5 Å of Tyr27 in the structure of SNase.[46,47] Interestingly, residue 27 is located in a β-turn connecting strands II and III of the β-barrel, whose amide groups are protected from H/D exchange early in refolding (within 10 ms).[37] In addition, turn regions are considered to be likely initiation sites in protein folding in general.[49,50] Thus, the observed decrease in fluorescence of Trp27 SNase on the submillisecond time scale provides evidence for rapid formation of the reverse turn

within the strand II–strand III hairpin, which brings Trp27 within close contact of a quenching partner, such as Lys28.

For five variants (Trp76, Trp91, Trp102, Trp121, and WT* SNase), the fluorescence of the I_2 state populated over the 10–100 ms time range is similar to or slightly higher than that of the I_1 intermediate (Table 4) and undergoes a major increase only during the main folding phase on the 100 ms time scale (Figure 3(a)). Thus, these tryptophan probes become progressively shielded from the solvent during folding and are fully buried upon formation of the native state (the M-state has negligible population during refolding and only affects the kinetics of unfolding). In the case of WT* SNase, the I_2 state is more fluorescent than the U and I_1 states, suggesting that the C-terminal region of helix H3 involving Trp140 is recruited to the structured regions at this stage of folding (~50 ms). In addition, previous H/D exchange results showed that stable hydrogen-bonded interactions begin to be formed between 10 and 100 ms, as indicated by protection factors larger than five for residues in strands II and III, as well as a residue in helix H3 (Lys134).[37] Despite the native-like secondary structure content of the I_2 state, based on the burst phase observed by far-UV CD,[41,43] the fluorescence of I_2 is closer to that of the unfolded rather than the native state, which gives rise to a lag phase in the appearance of the N-state (Figure 3 and Table 3), as previously reported for WT SNase and a proline-free variant.[40] Our present observation that two variants, Trp15 and Trp61 SNase, exhibit a distinct kinetic phase with a time constant matching that of the lag phase (~30 ms) provides striking confirmation for this mechanism. Thus, the lag phase reflects accumulation of the I_2 intermediate, which in the case of the Trp15 and Trp61 variants has a higher intrinsic fluorescence than all other states (Table 4), giving rise to a transient increase in fluorescence of these tryptophan residues before they encounter their quenching partners within the native structure. These observations further confirm that the I_1 and I_2 states are sequential intermediates along a direct path from the unfolded to the native state; if the native state could be reached rapidly along a parallel pathway, bypassing I_1 and I_2, this would give rise to a fast fluorescence change towards the native level, counteracting the lag phase or transient increase in fluorescence[51] (see also Roder *et al.*[5], and Kiefhaber[52] for further discussion). It should be noted that the $U' \Leftrightarrow I' \Leftrightarrow M$ branch of Scheme 1 does not provide a short-circuit, since the $I' \rightarrow M$ transition is slower than the rate-limiting ($I_2 \rightarrow M$) step along the main folding path.

The intrinsic fluorescence of Trp15 and Trp61 SNase is quenched after the rate-limiting step of the refolding reaction, indicating that the specific side-chain contact between these engineered tryptophan residues and their respective quenching partners (Lys24 and Gln106) is established only upon formation of the native state. The fact that a specific contact between Trp15 and Lys24, which are located on strands I and II of the β-sheet, respectively, is established after the rate-limiting folding step indicates that complete assembly of the β-barrel occurs only during the final stages of folding, long after formation of the strand II/strand III hairpin. The progressive increase in fluorescence in going from U through I_1 to I_2 observed for the Trp15 and Trp61 variants is attributed to partial burial of the side-chains in a hydrophobic environment within the collapsed molecule. In fact, a few hydrophobic residues, including Met26 (strand II) and Pro31 (turn between strands II and III), are in contact with Ile15 (strand I) in the crystal structure of H124L SNase.[47] Similarly, Phe61 located in helix H1 interacts with hydrophobic residues in helix H1 and H2 , including Met65 (helix H1), Val99 (helix H2) and Leu103 (helix H2). Thus, we suggest that the Trp15 and Trp61 side chains first encounter these hydrophobic residues upon formation of the I_1 and I_2 states, before they engage in specific contacts with the corresponding quenchers (Lys24 and Gln106, respectively). This conclusion is supported by our previous folding experiments on WT* and Trp76 SNase monitored by ANS,[24] and suggests that a loosely packed hydrophobic core is formed within the first 100 μs of refolding comprising a large fraction of the β-barrel domain as well as helix H1 and H2.

Taken together, the folding kinetics as monitored by the various tryptophan residues suggests a scenario in which the probes are initially buried in a collapsed, but loosely packed ensemble of states, followed by the rate-limiting formation of the densely packed native core mediated by specific tertiary-structural contacts, which bring the tryptophan residues into close contact with intramolecular quenchers. As in the case of other proteins of similar or larger size,[2] the folding mechanism of SNase exhibits several intermediate states populated along parallel folding channels. This kinetic complexity may be a manifestation of a "rough energy landscape", which can give rise to a large number of alternative pathways that eventually converge toward a common free energy minimum corresponding to the native structure.[53–56] According to this landscape view of protein folding, intermediates are thought to accumulate mainly as a result of kinetic trapping or topological frustration. It is quite possible that trapping of misfolded states is responsible for some of the minor species populated along parallel pathways during folding of SNase,[24,36,40] as well as other proteins.[21,52,57,58] However, the states populated along the main pathway exhibit features characteristic of productive folding intermediates, including progressive structural organization and increasing stability towards the later stages of folding. Although as many as six exponential phases are required to reproduce the fluorescence-detected time-course of folding (see Supplementary Data, Table 1), the individual phases are well resolved in time, and a simple kinetic scheme with a limited number of populated states is adequate to describe the kinetics. This "chemical kinetics" description can be consolidated with the energy landscape view of protein folding if the free energy

surface is subdivided into several regions (macrostates) mutually separated by substantial free energy barriers. The protein can rapidly explore conformational space within each region, which can comprise a broad ensemble of unfolded or partially folded states, but encounters larger kinetic barriers before entering another region of conformational space. This type of free energy surface can thus give rise to multi-exponential folding kinetics.

Materials and Methods

Expression plasmids containing WT* SNase or seven single-Trp variants (Trp15, Trp27, Trp61, Trp76, Trp91, Trp102 and Trp121 SNase) were prepared by using QuikChange Site-Directed mutagenesis kit (Stratagene, CA). The proteins were prepared and purified as described.[24,59] The extinction coefficients of the variants were determined as described by Pace *et al*.[60]

The thermal unfolding transitions of WT* SNase and its variants were measured by monitoring the change in far-UV CD at 222 nm on increasing the temperature from 15 °C to 80 °C. The data were recorded in 2 mm quartz cuvettes on an AVIV 62DS spectropolarimeter (Lakewood, NJ) equipped with a thermoelectric sample holder. The solutions contained ~10 μM protein, 25 mM sodium phosphate, 50 mM NaCl, 0.5 mM EDTA (pH 7.0).

Steady-state fluorescence emission spectra were recorded on a PTI (South Brunswick, NJ) QM-2000 spectrofluorometer. The wavelength at the emission maximum was obtained by non-linear least squares fitting of part of the fluorescence spectra using a Gaussian function. The solution contained 5 μM protein in 100 mM sodium acetate (pH 5.2) in the presence or absence of 2.4 M GuHCl, or in 20 mM phosphoric acid (pH 2.0). Samples were incubated for 5–15 min before each measurement at 15 °C.

Continuous-flow fluorescence measurements were carried out as described by Shastry *et al.*,[61] using a flow rate of 1.04 ml/s. Stopped-flow data were recorded on a BioLogic (Grenoble, France) SFM-4 instrument. The dead times of the continuous and stopped-flow devices were 100–120 μs and 2.4 ms, respectively. For refolding measurements by both continuous and stopped-flow techniques, stock solutions of acid-unfolded SNase variants were prepared in 20 mM phosphoric acid (pH 2.0). The refolding reaction was initiated by tenfold dilution of the acid-unfolded protein with refolding buffer containing 100 mM sodium acetate (pH 5.3). The time-dependent fluorescence change was monitored with a 324 nm high-pass filter, exciting Trp fluorescence at 288 nm using a monochromator with a 4 nm band pass. For quantitative modeling of the combined kinetic data, standard numeric methods[62] were used to solve the system of linear differential equations describing a particular kinetic scheme, using IGOR software to determine the eigenvalues and eigenvectors of the corresponding rate matrix as described.[24]

Acknowledgements

The work was supported by NIH grants R01 GM056250 and CA06927, and an appropriation from the Commonwealth of Pennsylvania to the Fox Chase Cancer Center. The Spectroscopy Support Facility provided access to fluorescence and CD spectrometers.

Supplementary Data

Supplementary data associated with this article can be found, in the online version, at doi:10.1016/j.jmb.2007.02.006

References

1. Baldwin, R. L. & Rose, G. D. (1999). Is protein folding hierarchic? II. Folding intermediates and transition states. *Trends Biochem. Sci.* **24**, 77–83.
2. Bilsel, O. & Matthews, C. R. (2000). Barriers in protein folding reactions. *Advan. Protein Chem.* **53**, 153–207.
3. Arai, M. & Kuwajima, K. (2000). Role of the molten globule state in protein folding. *Advan. Protein Chem.* **53**, 209–282.
4. Daggett, V. & Fersht, A. R. (2003). Is there a unifying mechanism for protein folding? *Trends Biochem. Sci.* **28**, 18–25.
5. Roder, H., Maki, K. & Cheng, H. (2006). Early events in protein folding explored by rapid mixing methods. *Chem. Rev.* **106**, 1836–1861.
6. Kuwajima, K., Yamaya, H., Miwa, S., Sugai, S. & Nagamura, T. (1987). Rapid formation of secondary structure framework in protein folding studied by stopped-flow circular dichroism. *FEBS Letters*, **221**, 115–118.
7. Kuwajima, K., Garvey, E. P., Finn, B. E., Matthews, C. R. & Sugai, S. (1991). Transient intermediates in the folding of dihydrofolate reductase as detected by far-ultraviolet circular dichroism spectroscopy. *Biochemistry*, **30**, 7693–7703.
8. Elöve, G. A., Chaffotte, A. F., Roder, H. & Goldberg, M. E. (1992). Early steps in cytochrome c folding probed by time-resolved circular dichroism and fluorescence spectroscopy. *Biochemistry*, **31**, 6876–6883.
9. Agashe, V. R., Shastry, M. C. R. & Udgaonkar, J. B. (1995). Initial hydrophobic collapse in the folding of barstar. *Nature*, **377**, 754–757.
10. Takahashi, S., Yeh, S.-R., Das, T. K., Chan, C.-K., Gottfried, D. S. & Rousseau, D. L. (1997). Folding of cytochrome *c* initiated by submillisecond mixing. *Nature Struct. Biol.* **4**, 44–50.
11. Chan, C.-K., Hu, Y., Takahashi, S., Rousseau, D. L., Eaton, W. A. & Hofrichter, J. (1997). Submillisecond protein folding kinetics studied by ultrarapid mixing. *Proc. Natl Acad. Sci. USA*, **94**, 1779–1784.
12. Shastry, M. C. R. & Roder, H. (1998). Evidence for barrier-limited protein folding kinetics on the microsecond time scale. *Nature Struct. Biol.* **5**, 385–392.
13. Shastry, M. C. R., Sauder, J. M. & Roder, H. (1998). Kinetic and structural analysis of submillisecond folding events in cytochrome *c*. *Acc. Chem. Res.* **31**, 717–725.
14. Park, S.-H., Shastry, M. C. R. & Roder, H. (1999). Folding dynamics of the B1 domain of protein G explored by ultrarapid mixing. *Nature Struct. Biol.* **6**, 943–947.
15. Akiyama, S., Takahashi, S., Ishimori, K. & Morishima, I. (2000). Stepwise formation of alpha-helices during cytochrome *c* folding. *Nature Struct. Biol.* **7**, 514–520.

16. Grigoryants, V. M., Veselov, A. V. & Scholes, C. P. (2000). Variable velocity liquid flow EPR applied to submillisecond protein folding. *Biophys. J.* **78**, 2702–2708.
17. Capaldi, A. P., Shastry, R. M. C., Kleanthous, C., Roder, H. & Radford, S. E. (2001). Ultra-rapid mxing experiments reveal that Im7 folds *via* an on-pathway intermediate. *Nature Struct. Biol.* **8**, 68–72.
18. Kuwata, K., Shastry, R., Cheng, H., Hoshino, M., Batt, C. A., Goto, Y. & Roder, H. (2001). Structural and kinetic characterization of early folding events in beta-lactoglobulin. *Nature Struct. Biol.* **8**, 151–155.
19. Teilum, K., Maki, K., Kragelund, B. B., Poulsen, F. M. & Roder, H. (2002). Early kinetic intermediate in the folding of acyl-CoA binding protein detected by fluorescence labeling and ultrarapid mixing. *Proc. Natl Acad. Sci. USA*, **99**, 9807–9812.
20. Akiyama, S., Takahashi, S., Kimura, T., Ishimori, K., Morishima, I., Nishikawa, Y. & Fujisawa, T. (2002). Conformational landscape of cytochrome *c* folding studied by microsecond-resolved small-angle x-ray scattering. *Proc. Natl Acad. Sci. USA*, **99**, 1329–1334.
21. Gianni, S., Travaglini-Allocatelli, C., Cutruzzola, F., Brunori, M., Shastry, M. C. & Roder, H. (2003). Parallel pathways in cytochrome *c*(551) folding. *J. Mol. Biol.* **330**, 1145–1152.
22. Khan, F., Chuang, J. I., Gianni, S. & Fersht, A. R. (2003). The kinetic pathway of folding of barnase. *J. Mol. Biol.* **333**, 169–186.
23. Mayor, U., Guydosh, N. R., Johnson, C. M., Grossmann, J. G., Sato, S., Jas, G. S. *et al.* (2003). The complete folding pathway of a protein from nanoseconds to microseconds. *Nature*, **421**, 863–867.
24. Maki, K., Cheng, H., Dolgikh, D. A., Shastry, M. C. & Roder, H. (2004). Early events during folding of wild-type Staphylococcal nuclease and a single-tryptophan variant studied by ultrarapid mixing. *J. Mol. Biol.* **338**, 383–400.
25. Welker, E., Maki, K., Shastry, M. C., Juminaga, D., Bhat, R., Scheraga, H. A. & Roder, H. (2004). Ultrarapid mixing experiments shed new light on the characteristics of the initial conformational ensemble during the folding of ribonuclease A. *Proc. Natl Acad. Sci. USA*, **101**, 17681–17686.
26. Uzawa, T., Akiyama, S., Kimura, T., Takahashi, S., Ishimori, K., Morishima, I. & Fujisawa, T. (2004). Collapse and search dynamics of apomyoglobin folding revealed by submillisecond observations of α-helical content and compactness. *Proc. Natl Acad. Sci. USA*, **101**, 1171–1176.
27. Garcia, P., Bruix, M., Rico, M., Ciofi-Baffoni, S., Banci, L., Ramachandra Shastry, M. C. *et al.* (2005). Effects of heme on the structure of the denatured state and folding kinetics of cytochrome *b*(562). *J. Mol. Biol.* **346**, 331–344.
28. Bilsel, O., Kayatekin, C., Wallace, L. A. & Matthews, C. R. (2005). A microchannel solution mixer for studying microsecond protein folding reactions. *Rev. Sci. Instr.* **76**, 014302-1–014302-8.
29. Apetri, A. C., Maki, K., Roder, H. & Surewicz, W. K. (2006). Early intermediate in human prion protein folding as evidenced by ultrarapid mixing experiments. *J. Am. Chem. Soc.* **128**, 11673–11678.
30. Roder, H. & Wüthrich, K. (1986). Protein folding kinetics by combined use of rapid mixing techniques and NMR observation of individual amide protons. *Proteins: Struct. Funct. Genet.* **1**, 34–42.
31. Udgaonkar, J. B. & Baldwin, R. L. (1988). NMR evidence for an early framework intermediate on the folding pathway of ribonuclease A. *Nature*, **335**, 694–699.
32. Roder, H., Elöve, G. A. & Englander, S. W. (1988). Structural characterization of folding intermediates in cytochrome *c* by H-exchange labelling and proton NMR. *Nature*, **335**, 700–704.
33. Miranker, A., Robinson, C. V., Radford, S. E., Aplin, R. T. & Dobson, C. M. (1993). Detection of transient protein folding populations by mass spectrometry. *Science*, **262**, 896–899.
34. Nishimura, C., Dyson, H. J. & Wright, P. E. (2005). Enhanced picture of protein-folding intermediates using organic solvents in H/D exchange and quench-flow experiments. *Proc. Natl Acad. Sci. USA*, **102**, 4765–4770.
35. Chen, Y. & Barkley, M. D. (1998). Toward understanding tryptophan fluorescence in proteins. *Biochemistry*, **37**, 9976–9982.
36. Kamagata, K., Sawano, Y., Tanokura, M. & Kuwajima, K. (2003). Multiple parallel-pathway folding of proline-free Staphylococcal nuclease. *J. Mol. Biol.* **332**, 1143–1153.
37. Walkenhorst, W. F., Edwards, J. A., Markley, J. L. & Roder, H. (2002). Early formation of a beta hairpin during folding of staphylococcal nuclease H124L as detected by pulsed hydrogen exchange. *Protein Sci.* **11**, 82–91.
38. Nishimura, C., Riley, R., Eastman, P. & Fink, A. L. (2000). Fluorescence energy transfer indicates similar transient and equilibrium intermediates in staphylococcal nuclease folding. *J. Mol. Biol.* **299**, 1133–1146.
39. Maki, K., Ikura, T., Hayano, T., Takahashi, N. & Kuwajima, K. (1999). Effects of proline mutations on the folding of staphylococcal nuclease. *Biochemistry*, **38**, 2213–2223.
40. Walkenhorst, W. F., Green, S. M. & Roder, H. (1997). Kinetic evidence for folding and unfolding intermediates in Staphylococcal nuclease. *Biochemistry*, **63**, 5795–5805.
41. Kalnin, N. N. & Kuwajima, K. (1995). Kinetic folding and unfolding of Staphylococcal nuclease and its six mutants studied by stopped-flow circular dichroism. *Proteins: Struct. Funct. Genet.* **23**, 163–176.
42. Jacobs, M. D. & Fox, R. O. (1994). Staphylococcal nuclease folding intermediate characterized by hydrogen exchange and NMR spectroscopy. *Proc. Natl Acad. Sci. USA*, **91**, 449–453.
43. Sugawara, T., Kuwajima, K. & Sugai, S. (1991). Folding of staphylococcal nuclease A studied by equilibrium and kinetic circular dichroism spectra. *Biochemistry*, **30**, 2698–2706.
44. Becktel, W. J. & Schellman, J. A. (1987). Protein stability curves. *Biopolymers*, **26**, 1859–1877.
45. Woody, R. W. (2004). Circular dichroism of protein-folding intermediates. *Methods Enzymol.* **380**, 242–285.
46. Hynes, T. R. & Fox, R. O. (1991). The crystal structure of staphylococcal nuclease refined at 1.7 Å resolution. *Proteins: Struct. Funct. Genet.* **10**, 92–105.
47. Tuckses, D. M., Somoza, J. R., Prehoda, K. E., Miller, S. C. & Markley, J. L. (1996). Coupling between *trans/cis* proline isomerization and protein stability in staphylococcal nuclease. *Protein Sci.* **5**, 1907–1916.
48. Roder, H., Maki, K., Cheng, H. & Shastry, M. C. (2004). Rapid mixing methods for exploring the kinetics of protein folding. *Methods*, **34**, 15–27.
49. Wright, P. E., Dyson, H. J. & Lerner, R. A. (1988). Conformation of peptide fragments of proteins in solution: implications for initiation of protein folding. *Biochemistry*, **27**, 7167.

50. Freund, S. M. V., Wong, K.-B. & Fersht, A. R. (1996). Initiation sites of protein folding by NMR analysis. *Proc. Natl Acad. Sci. USA*, **93**, 10600–10603.
51. Capaldi, A. P., Kleanthous, C. & Radford, S. E. (2002). Im7 folding mechanism: misfolding on a path to the native state. *Nature Struct. Biol.* **9**, 209–216.
52. Kiefhaber, T. (1995). Kinetic traps in lysozyme folding. *Proc. Natl Acad. Sci. USA*, **92**, 9029–9033.
53. Bryngelson, J. D., Onuchic, J. N., Socci, N. D. & Wolynes, P. G. (1995). Funnels, pathways, and the energy landscape of protein folding: a synthesis. *Proteins: Struct. Funct. Genet.* **21**, 167–195.
54. Dobson, C. M. & Karplus, M. (1999). The fundamentals of protein folding: bringing together theory and experiment. *Curr. Opin. Struct. Biol.* **9**, 92–101.
55. Onuchic, J. N. & Wolynes, P. G. (2004). Theory of protein folding. *Curr. Opin. Struct. Biol.* **14**, 70–75.
56. Thirumalai, D. & Klimov, D. K. (2007). Intermediates and transition states in protein folding. *Methods Mol. Biol.* **350**, 277–303.
57. Iwakura, M., Jones, B. E., Falzone, C. J. & Matthews, R. C. (1993). Collapse of parallel folding channels in dihydrofolate reductase from *Escherichia coli* by site-directed mutagenesis. *Biochemistry*, **32**, 13566–13574.
58. Bilsel, O., Zitzewitz, J. A., Bowers, K. E. & Matthews, C. R. (1999). Folding mechanism of the alpha-subunit of tryptophan synthase, an alpha/beta barrel protein: global analysis highlights the interconversion of multiple native, intermediate, and unfolded forms through parallel channels. *Biochemistry*, **38**, 1018–1029.
59. Royer, C. A., Hinck, A. P., Loh, S. N., Prehoda, K. E., Peng, X., Jonas, J. & Markley, J. L. (1993). Effects of amino acid substitutions on the pressure denaturation of Staphylococcal nuclease as monitored by fluorescence and nuclear magnetic resonance spectroscopy. *Biochemistry*, **32**, 5222–5232.
60. Pace, C. N., Vajdos, F., Fee, L., Grimsley, G. & Gray, T. (1995). How to measure and predict the molar absorption coefficient of a protein. *Protein Sci.* **4**, 2411–2423.
61. Shastry, M. C. R., Luck, S. D. & Roder, H. (1998). A continuous-flow capillary mixer to monitor reactions on the microsecond time scale. *Biophys. J.* **74**, 2714–2721.
62. Berberan-Santos, M. N. & Martinho, J. M. G. (1990). The integration of kinetic rate equations by matrix methods. *J. Chem. Educ.* **67**, 375–379.
63. Kraulis, P. J. (1991). MOLSCRIPT: a program to produce both detailed and schematic plots of protein structures. *J. Appl. Crystallog.* **24**, 946–950.

Edited by C. R. Matthews

(Received 30 November 2006; received in revised form 31 January 2007; accepted 2 February 2007)
Available online 9 February 2007